Designing Gel Polymer Electrolyte with Synergetic Properties for Rechargeable Magnesium Batteries

Liping Wang [a,*], Zhenyou Li [a], Zhen Meng [a], Yanlei Xiu [a], Bosubabu Dasari [a],
Zhirong Zhao-Karger [a,b,*], Maximilian Fichtner [a,b,*]

[a] Helmholtz Institute Ulm (HIU) Electrochemical Energy Storage Helmholtzstrasse 11, D−89081, Ulm, Germany

[b] Institute of Nanotechnology (INT) Karlsruhe Institute of Technology (KIT) Hermann-von-Helmholtz-Platz 1, Eggenstein-Leopoldshafen, D-76344, Germany

ARTICLE INFO

ABSTRACT

Magnesium (Mg) batteries represent a promising candidate for energy-dense, sustainable and safe energy storage. However, the realization of practical Mg batteries remains challenging and advanced material design strategies are imperatively necessary. Herein, a novel magnesium tetrakis(hexafluoroisopropyloxy)borate-based non-corrosive gel polymer electrolyte has been synthesized by an *in-situ* polymerization. This gel polymer electrolyte exhibits unprecedented electrolytic properties in terms of high ionic conductivity (10^{-3} S cm^{-1}), reversible Mg plating/stripping capability (Coulombic efficiency ∼99%, 1000 cycles) and low voltage polarization. Simultaneously, the polymeric matrix can prevent dissolution and diffusion of soluble electrode materials. For the first time, the employment of a gel polymer electrolyte to suppress the polysulfide shuttle in Mg−S batteries has been demonstrated. Moreover, it can be extended to other polymer backbones and incorporated with other cathodes for improving battery performance.

1. Introduction

Recent research has witnessed rapid progress in a new scheme of multivalent ion batteries, which are based on the reversible inser tion of Mg^{2+}, Zn^{2+}, Al^{3+}, Ca^{2+} or hybrid ions. Among them, mag nesium battery with Mg metal anode is one of the most promising candidates, because of the merits of Mg metal in terms of high natu ral abundance (the 8th and 3rd most abundant element in the earth's crust and sea water, respectively), ambient stability and a high the oretical volumetric capacity (3832 mA h cm^{-3}) [1 8]. Nevertheless, the development of magnesium battery is hindered by the difficulty of finding proper electrolytes. Cl containing electrolyte solutions based on Grignard reagents have been explored in the early stages [9 14], but they suffer from certain drawbacks, including relatively low an odic stability, limited chemical compatibility with cathode materials and severe corrosion to the metallic cell components. Hence, more and more research interests have been devoted to formulating Cl free simple Mg ion conductive salt based electrolytes. For instance, non corrosive magnesium monocarborane ($Mg(CB_{11}H_{12})_2$) salt [15], magnesium hex afluoroisopropylaluminate ($Mg[Al(hfip)_4]$) salt [16] and magnesium tetra(trifluoroethanoloxy)borate ($Mg[B(Otfe)_4]_2$) salt [17] based elec trolyte. All of them have high anodic stability up to 3V.

Recently developed magnesium tetrakis (hexafluoroisopropyloxy) borate $Mg[B(hfip)_4]_2$ ($hfip = OC(H)(CF_3)_2$) electrolytes exhibit out standing electrochemical performance and good chemical compatibility [18]. Highly reversible sulfur redox mechanism and discharge/charge chemistry with this non corrosive electrolyte have been demonstrated [19]. Nevertheless, Mg S batteries with a liquid electrolyte are still confronting critical issues correlated with the dissolution of the sulfur species during the discharging/charging process [9,20,21]. During the discharge process, solid state sulfur can be reduced to the long chain polysulfide, which may dissolve in the liquid electrolyte and diffuse across the separator to the anode side, where they can be further re duced. This so called polysulfide shuttle leads to a low active material utilization and short cell life [22 25]. In particular, it has been unveiled that the Mg S batteries show high tendency of fast self discharge in the conventional liquid electrolytes, leading to serious capacity loss from the initial cycles [24,26,27]. Similarly, dissolution of active material in liquid electrolyte is one of the most crucial challenges in the exploration of organic electrode materials for high energy Mg batteries [28 31].

The development of gel polymer electrolytes (GPEs) may provide a promising solution to circumvent the above concerns. GPE with favor able electrochemical properties can be used as a competitive alterna tive for improving battery performance, which exhibits additional ad vantages of improved safety (less internal short circuit and less elec

* Corresponding authors.

E-mail addresses: liping.wang@partner.kit.edu (L. Wang), zhirong.zhao-karger@kit.edu (Z. Zhao-Karger), m.fichtner@kit.edu (M. Fichtner).

trolyte leakage) and mechanical durability of electrochemical devices [32,33]. Additionally, some built in functions can be integrated in a polymer electrolyte, providing an efficient approach for improving bat tery performance. Taking into account the intrinsically low mobility of Mg2+ ion, a GPE designed by trapping solvent molecules in a polymer ized gel network may retain adequate Mg ion conductivity and at the same time limit the dissolution and diffusion of soluble electrode ma terials. For Mg−S batteries, the utility of GPE can be an efficient ap proach to inhibit the diffusion of the polysulfides. Some research ef forts have been taken for Mg polymer electrolytes such as the combi nations of polymers including poly(ethylene oxide) (PEO) and copoly mer PVDF−HFP with $Mg(ClO_4)_2$ or MgTFSI$_2$ salt [34 41]. However, the inferior electrochemical properties and ion transport capability of these polymer electrolytes hinder their implementation in Mg batteries. Recently, polytetrahydrofuran (PTHF) is reported to establish a GPE, which shows an excellent Mg anode compatibility and high conductiv ity [33]. However, as authors mentioned, MgCl$_2$ may reduce the anodic stability of electrolyte system and the corrosive nature of the Cl based electrolytes limit their practical application. Thus, developing Cl free gel polymer electrolytes is of great need. The reported PTHF based gel poly mer electrolyte achieved a promising performance with Mo_6S_8 cathode, but the performance of gel polymer electrolyte in Mg S system was not reported. To the best of our knowledge, there are only few reports about gel polymer electrolytes for Mg−S batteries [42,43].

In this work, a novel Cl free $Mg[B(hfip)_4]_2$ (MgBOR) based gel poly mer electrolyte was synthesized by an *in situ* polymerization. Inspired by the previous report, we first choose the PTHF backbone to build the GPE. The MgBOR−PTHF−GPE was used as a rational substitute for the conventional liquid electrolyte in Mg S batteries. For the first time, a gel polymer electrolyte is presented, which allows reversible Mg plat ing/stripping and is compatible with the sulfur cathode. The GPE was prepared during the cell assembly and exhibited superior electrochemi cal performance in both symmetric/asymmetric cells and in Mg−S bat tery cells. Impedance analyses and post mortem electron microscopic tests demonstrated that the MgBOR−PTHF−GPE can mitigate the safety hazards and suppress the shuttle effect of polysulfide. To further verify this concept, the $Mg[B(hfip)_4]_2$ based GPE was extended to the other polymer backbone with polymerized pentaerythritol tetraacrylate (PE TEA). These findings indicate the promising features of the Cl free gel polymer electrolyte for practical Mg−S battery chemistry.

2. Results and Discussion

2.1. Preparation and characterization

Fig. 1a shows the schematic process for preparing the MgBOR−PTHF−GPE. $Mg(BH_4)_2$ was used as an initiator for the polymerization of PTHF and the liquid $Mg[B(hfip)_4]_2$ electrolyte in dimethoxyethane (DME) was transformed to the quasi solid GPE by *in−situ* polymerization. The MgBOR−PTHF−GPE obtained from polymerization was characterized by X−ray diffraction (XRD) measure ments as shown in **Fig. S1**a. After polymerization, the crystalline peaks belonging to PTHF and MgBOR disappeared, implying the amorphous phase of MgBOR−PTHF−GPE, which was further characterized by Fourier transform infrared spectra (FT−IR) (Figure S1b). The peaks in the range of 3000 2600 cm^{-1} (C H stretch) reflect the contributions from DME or PTHF. The band at ~3450 cm^{-1} (O H stretch) suggests the existence of a terminating hydroxyl functional group in PTHF. The terminating hydroxyl group was consumed during polymerization, and thus it is disappeared from the GPE spectrum. These results confirm that the PTHF has been further polymerized, indicating the formation of GPE. Thermogravimetric analysis (TGA) and differential scanning calorimetry (DSC) were carried out to evaluate the thermal stability of MgBOR−PTHF−GPE under argon atmosphere (Figure S1c). The DSC profile reveals that the GPE started to melt with partial desolvation of DME at around 108 °C, as indicated by the endothermic peak. A

sharp decline was observed at 135 °C, which is due to the degradation of PTHF backbone and further decomposition of the MgBOR. For comparison, the TGA result of pure MgBOR salt is also shown in Figure S1d. The salt started to release most of the DME and decomposes at about 150 °C, which is consistent with our previous report [18]. In addition, the morphology and microstructure of separators with or without GPE were characterized by SEM (**Fig. S2-3**). As shown in the SEM images, the glass fiber (with a diameter of ≈ 1 μm) act as the scaffold, in which MgBOR−PTHF−GPE was filled. The glass fiber provides mechanical support while the MgBOR−PTHF−GPE offers the pathway for ionic transport. EDS maps demonstrate that C, O, Si, Al, Mg, and F are homogeneously distributed throughout the separator with MgBOR−PTHF−GPE. Compared with the blank separator, additional el ement Mg is derived from both $Mg[B(hfip)_4]_2$ and $Mg(BH_4)_2$, while F is from $Mg[B(hfip)_4]_2$. Apart from that, the corresponding cross sectional SEM maps of the GPE coated separator are demonstrated in Fig. 1c g, which further manifest that the separator membrane was homogenously infiltrated with MgBOR−PTHF−GPE. The optical photograph of the synthesized MgBOR−PTHF−GPE is displayed in Fig. 1h.

Ionic conductivity is a key parameter to evaluate the GPE and is of prominent importance to achieve high rate capability. The ionic con ductivity of the MgBOR−PTHF−GPE was measured by electrochemical impedance spectroscopy (EIS) in a symmetrical stainless steel (SS) two electrode device at 25°C (Fig. 2a). Based on the EIS fitting results (Fig. 2b), the conductivity was calculated to be 2.01 (± 0.02) mS cm^{-1}. To the best of our knowledge, it is the highest value among the re ported Mg polymer electrolytes and even comparable with some liq uid electrolytes [20,33,36 40,44 46]. The high ionic conductivity of MgBOR−PTHF−GPE may be attributed to the unique chemical struc ture of $Mg[B(hfip)_4]_2$ and the ether bond rich high polymerized matrix. Such high ionic conductivity is also in accordance with the good rate performance of the symmetric cell in the following part. Another im portant feature for electrolyte is the Mg^{2+} transference number (t_{Mg}^{2+}), which quantifies the fraction of ionic transport. The transference num ber of the MgBOR−PTHF−GPE was determined using the steady state current method from Bruce and Vincent [47]. AC impedance of the cell was measured both before and after the voltage polarization, and the Nyquist plots obtained are shown in the inset of Fig. 2c. The values of the electrode electrolyte interfacial resistances were obtained from these Nyquist plots. The t_{Mg}^{2+} of MgBOR−PTHF−GPE was determined to be 0.300±0.02, which is notably comparable with those of the exist ing polymer electrolytes for Li ion batteries [33,37,44]. The anodic sta bility of the GPE was assessed by linear sweep voltammetry (LSV) using SS as a working electrode. A comparatively high anodic stability of 2.57 V vs. Mg/Mg^{2+} was observed when the current increased to 0.01 mA (**Fig. S4**). The magnesium deposition and stripping process on the Mg electrode surface was confirmed through cyclic voltammetry (CV) with a two electrode SS//MgBOR−PTHF−GPE//Mg cell at 25°C (Fig. 2d). The cathodic and anodic peaks could be detected, denoting the magnesium deposition and stripping, respectively. In the first cycle, the potential interval between the onset potential for Mg plating and Mg stripping is around 1.0 V. In the following cycles, the current increase and the volt age polarization decrease gradually, which indicate faster kinetics and better reversibility. Furthermore, a long time Mg plating/stripping be havior was also achieved in a SS//MgBOR−PTHF−GPE//Mg cell with a plating time of 0.5 h (Figure 2e). From the 10th cycle, the cell showed a consistent and high Coulombic efficiency at 99%, which remained sta ble even after 1000 stripping/plating cycles (Fig. 2f). This long term performance even outperforms conventionally used liquid electrolyte [11,48]. In addition, the surface morphology and composition of the SS electrode after stripping/plating was scrutinized by *ex situ* SEM analy sis (Inset). Mg element was observed with the elemental map, confirm ing that Mg was tightly packed and agglomerated on the SS substrate. The magnesiumdeposits on Mg anode after 150 cycles are agglomerated without severe pulverization and cracks with MgBOR−PTHF−GPE. (**Fig. S5**), which confirms the stable plating/stripping behavior.
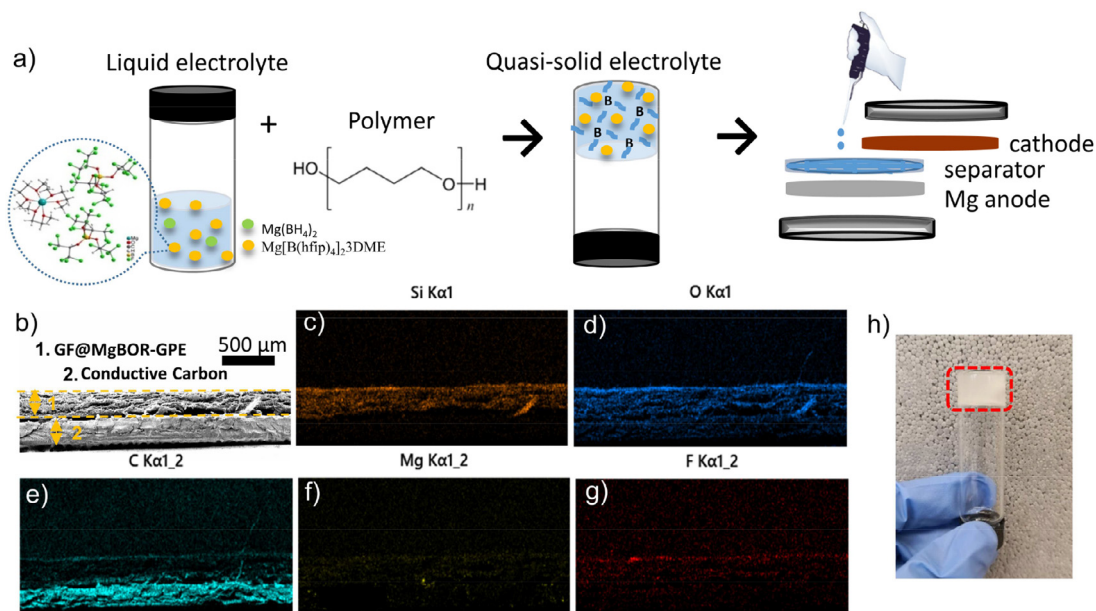
Fig. 1. (a) Schematic illustration of the preparation for the MgBOR−PTHF−GPE. The cross-section (b) SEM image and (c-g) EDS maps of glass fiber membrane coated with dry MgBOR−PTHF−GPE. (h) Optical photographs of synthesized MgBOR−PTHF−GPE.
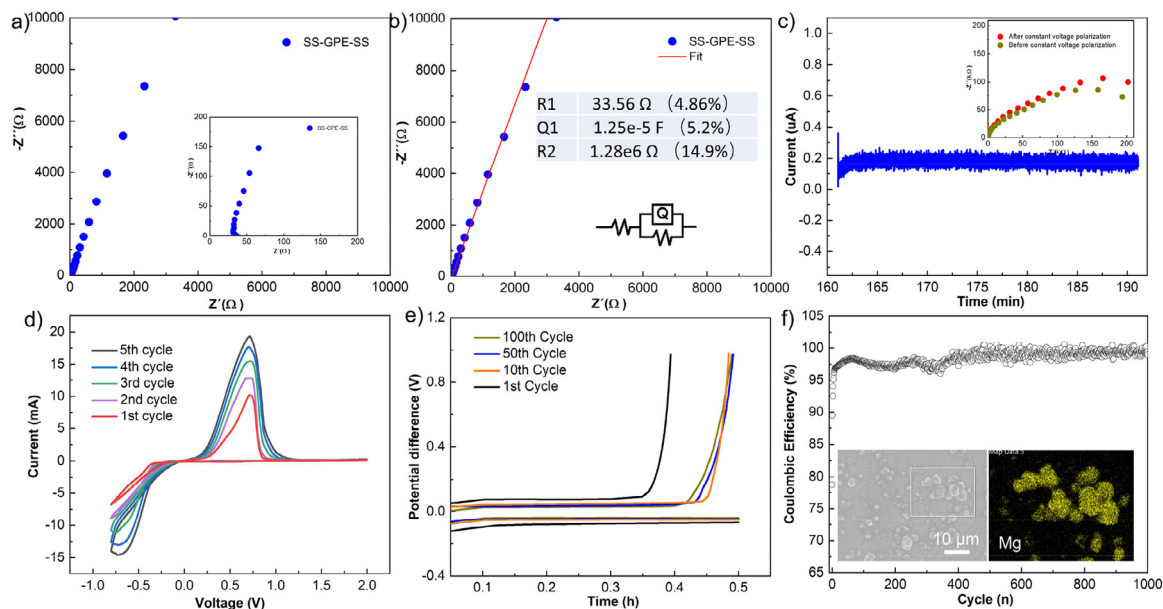

Fig. 2. (a–b) Electrical impedance spectroscopy and the corresponding fitting result of SS//MgBOR−PTHF−GPE//SS cell at 25 °C. (c) DC polarization curve of the symmetrical Mg//MgBOR−PTHF−GPE//Mg cell with a total applied potential difference of 0.02 V (Inset shows Nyquist plots of the symmetrical cell before and after DC polarization.). (d) Current–voltage curves for Mg plating and stripping in MgBOR−PTHF−GPE at a sweep rate of 5 mV s^{-1}. (e) Mg plating and stripping profiles of the SS//MgBOR−PTHF−GPE//Mg cell in MgBOR−PTHF−GPE and (f) the corresponding Coulombic efficiency as a function of cycle number. The current density is 0.1 mA cm^{-2} (Inset: SEM image and EDS map for Mg of a SS disc collected from a SS//MgBOR−PTHF−GPE//Mg cell in MgBOR−PTHF−GPE after stripping/plating for 150 cycles).Galvanostatic cycling tests with MgBOR−PTHF−GPE were also investigated in a symmetric cell to provide more evidence of the reversible nature of the Mg plating/stripping in the GPE. Fig. 3a shows the overpotential values carried out at different current densities from 0.05 to 0.50 mA cm^{-2}. The deposition/stripping overpotential increased slightly with the areal current densities and became stable after few cycles. Even at the relatively high current of 0.50 mA cm^{-2}, the cell could persevere a low polarization of about 0.055V. A long-term cyclability test with a current of 0.1 mA cm^{-2} is shown in Fig. 3b. The Mg symmetrical cell continues to operate stably beyond 500 cycles while keeping a low polarization below 0.06 V. It should be noted that this performance is comparable with the most recent state-of-the-art liquid electrolytes. [11,49,50] Such excellent cycling performance up to 500 cycles is unique comparing to existing Mg-ion-conducting polymer electrolytes. [37] Furthermore, the morphology of the Mg disc after cycling is shown in **Fig. S6**. Long−term cycling performance at a high current density of 0.5 mA cm^{-2} was also tested and is demonstrated in **Fig. S7**. At high current density, the cell still presented excellent cyclic stability. Besides, its overpotential remained at 0.135V even after 500 cycles. All these results demonstrate that an efficient plating/stripping of Mg can be realized successfully with small overpotential by using MgBOR−PTHF−GPE.
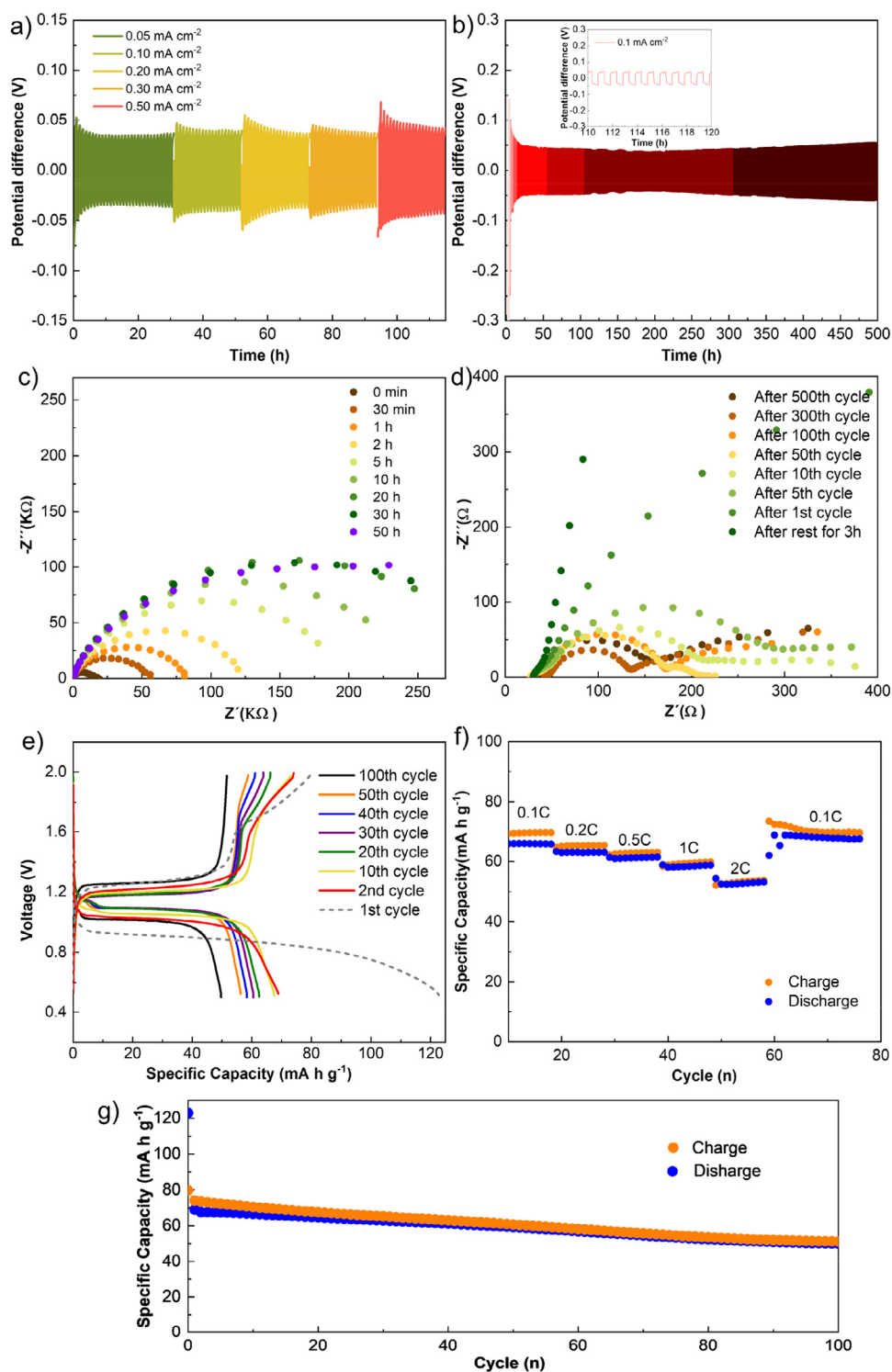
Fig. 3. (a) The polarization properties of Mg symmetrical cell at various current densities (from 0.05 mA cm^{-2} to 0.5 mA cm^{-2}) for a plating/stripping time of 0.5 h. (b) Long-term cycling of Mg symmetrical cell using MgBOR−PTHF−GPE. The current density is 0.1 mA cm^{-2} and 0.05 mA h cm^{-2} Mg is plated and stripped per cycle. Insets: enlarged profiles at the 110 to 120 cycle numbers noted. Nyquist plots of the Mg symmetrical cell with MgBOR−PTHF−GPE (c) with different rest times at OCV or (d) after different cycle numbers. (e) Galvanostatic discharge/charge voltage profiles of Mo$_6$S$_8$//MgBOR−PTHF−GPE//Mg cells at 25 °C. (f) Rate performance of the battery with the current density ranges from 0.1C to 2C. (e) Cycling performance of Mo$_6$S$_8$//MgBOR−PTHF−GPE//Mg cells at a current density of 0.1C.

To gain further understanding of the origin of excellent cycling stability, EIS was monitored with the cell during various rest times at the open circuit voltage (OCV) and after different galvanostatic cycles. Fig. 3c displays the Nyquist plots measured at OCV. The impedance was measured to be around 17 kΩ after assembling the cell, and the impedance was observed to increase incrementally with the rest time and became stable at around 289 kΩ after 20 h. This phenomenon has been reported in previous literature [19,51]. The increasing resistance on the Mg electrode may result from an adsorption layer from the solvent. Apart from that, there is another possibility that a kind of solid electrolyte inter

phase might form with this GPE. The interfacial resistance decreased dramatically after cycling. As shown in Fig. 3d, the impedance was found to be approximately 200 Ω after 50 cycles at 0.1 mA cm^{-2}, and even lower resistances around 95 Ω and 124 Ω were achieved after 300 and 500 cycles. We assume that the high impedance of the cells with the MgBOR−PTHF−GPE after the long rest periods might derive from the adsorption layer on the Mg surface, which shows no additional impediment after cycling [52]. Both the low interfacial impedance and the good interfacial compatibility contribute to the excellent electrochemical stability as discussed above. The MgBOR−PTHF−GPE have
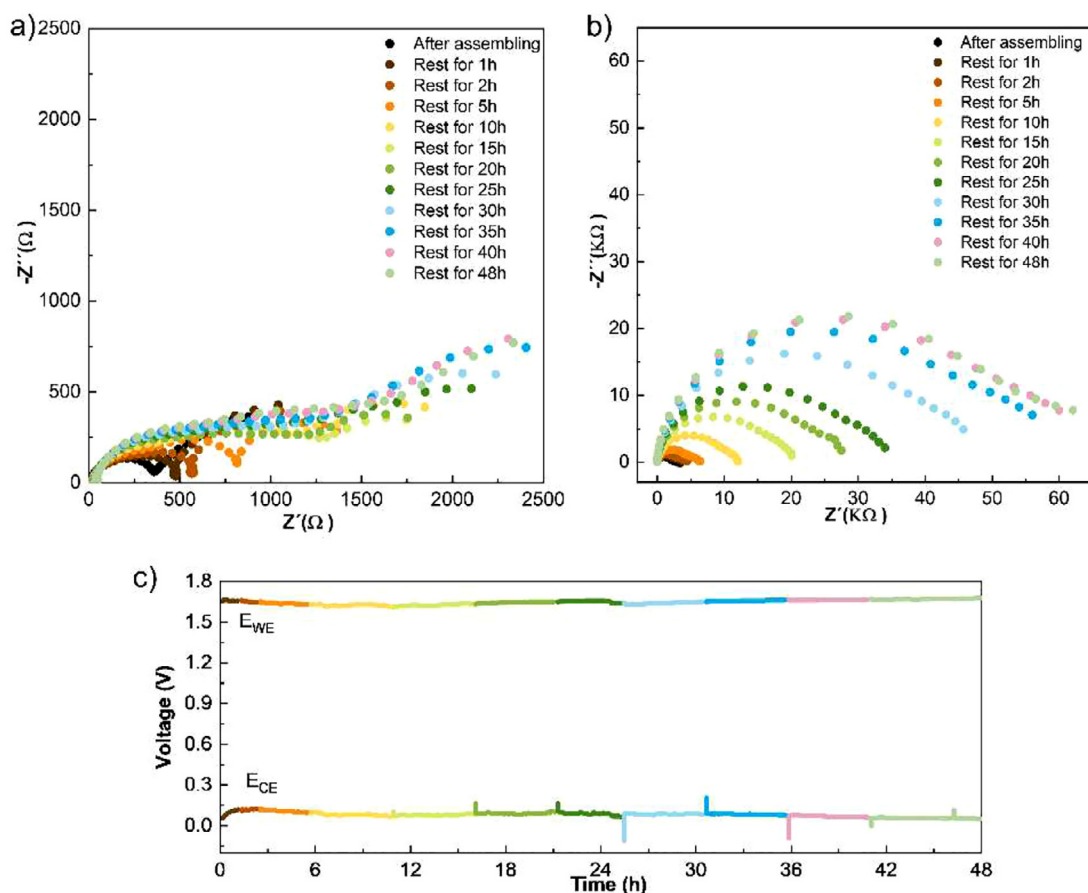
Fig. 4. Changes in the impedance spectra of (a) ACC/S cathode and (b) Mg anode of the Mg−S cell rest for 48 h at the frequency range of 1 MHz to 10 mHz. (c) Potential profiles of the Mg−S cell kept at OCV for 48 h.

succeeded utilized with the benchmark cathode Chevrel phase Mo_6S_8 to show its suitability for Mg batteries. **Fig. S8** shows the XRD patterns and SEM results of the Mo_6S_8 cathode material. The electrochemical performance of the cell is presented in Fig. 3e g, indicating a good rate capability and an impressive cycling performance. At a current density of 0.1C, after 100 cycles the specific capacity still maintained at 50.1 mA h g^{-1}. The corresponding CV profiles and EIS results during cycling are also demonstrated in **Fig. S9**. In addition, from previous report, Mg batteries require activation cycles for Mg plating/stripping with liquid Mg[B(hfip)$_4$]$_2$ electrolyte [18,53]. The activation process lasted for sev eral cycles with a simultaneous increase in the cell capacity. Here, from the first cycle the highest discharge capacity was already observed with out any activation cycles with the GPE. It could be explained that, small amount of Mg(BH$_4$)$_2$ may remain unreacted after polymerization. The reductive BH$_4^-$ could remove the thin oxide layer on the Mg anode and may boost the active process during cycling [53]. It is also very im portant to optimize the amount of the Mg(BH$_4$)$_2$ inside the electrolyte. These results show that the MgBOR−PTHF−GPE is well suited for use in Mg batteries.

2.2. MgBOR−PTHF−GPE for Mg−S batteries

The activated carbon cloth based sulfur cathodes (ACC/S) were fab ricated via a commonly used melt diffusion method. The SEM and EDS images of ACC/S in **Fig. S10** demonstrate that sulfur was evenly and completely dispersed into the porous carbon fibers. The changes in the OCV and corresponding impedances of the cell have been investigated by monitoring separately the cathode and anode potentials over a rest ing period of 48 h with a three electrode cell as shown in Fig. 4. Here ACC/S works as the working electrode (WE), Mg foil as the counter elec

trode (CE), and Mg ring as the reference electrode (RE), respectively. During 48 h of the resting period, the cathode potential increased from 1.62 V to 1.64 V. Besides, on the anode side, the initial potential was 0.053 V and the potential stabilized at 0.052 V after 48 h. In contrast, with the common liquid electrolyte, Mg−S batteries always suffer from serious self discharge behavior [26,27]. The stable OCV validates that the MgBOR−PTHF−GPE can effectively suppress the dissolution as well as the diffusion of polysulfide, and thus protect the anode from side reactions with the dissolved sulfur species and inhibit the battery self discharge. Both the cathode and anode impedance increased during the resting time, especially the anode side, which may be related to an ad sorption layer formation on the Mg surface mentioned before. After sev eral hours, the impedance became stable, which indicates the interface between GPE and electrode was stabilized. SEM was used to charac terize the Mg anode after disassembling the cell (**Fig. S11**). From the SEM results, almost no morphological change was observed. EDS result demonstrates that Mg was homogeneously distributed with additional elements C and O, which may be generated by a short exposition to air.

The electrochemical performances of Mg S cells with liquid or gel electrolytes after aging were investigated using coin cells. **Fig. 5**a b show the galvanostatic discharge/charge profiles of the cells with liq uid or gel electrolytes. In the first cycle, the cell with liquid electrolyte exhibited a discharge capacity of 320.9 mA h g^{-1} with a Coulombic efficiency of 61.9%. In contrast, the cell with GPE delivered both a higher discharge capacity (741.1 mA h g^{-1}) and a higher Coulombic effi ciency (97.2%). The significant capacity fade and decrease of discharge potential in the liquid electrolyte indicate the serious self discharge caused by the polysulfide problem. After 20 cycles, the discharge ca pacity decreased to 186.3 mA h g^{-1} with liquid electrolyte. While with GPE the discharge capacity remained over 500 mA h g^{-1}, almost three
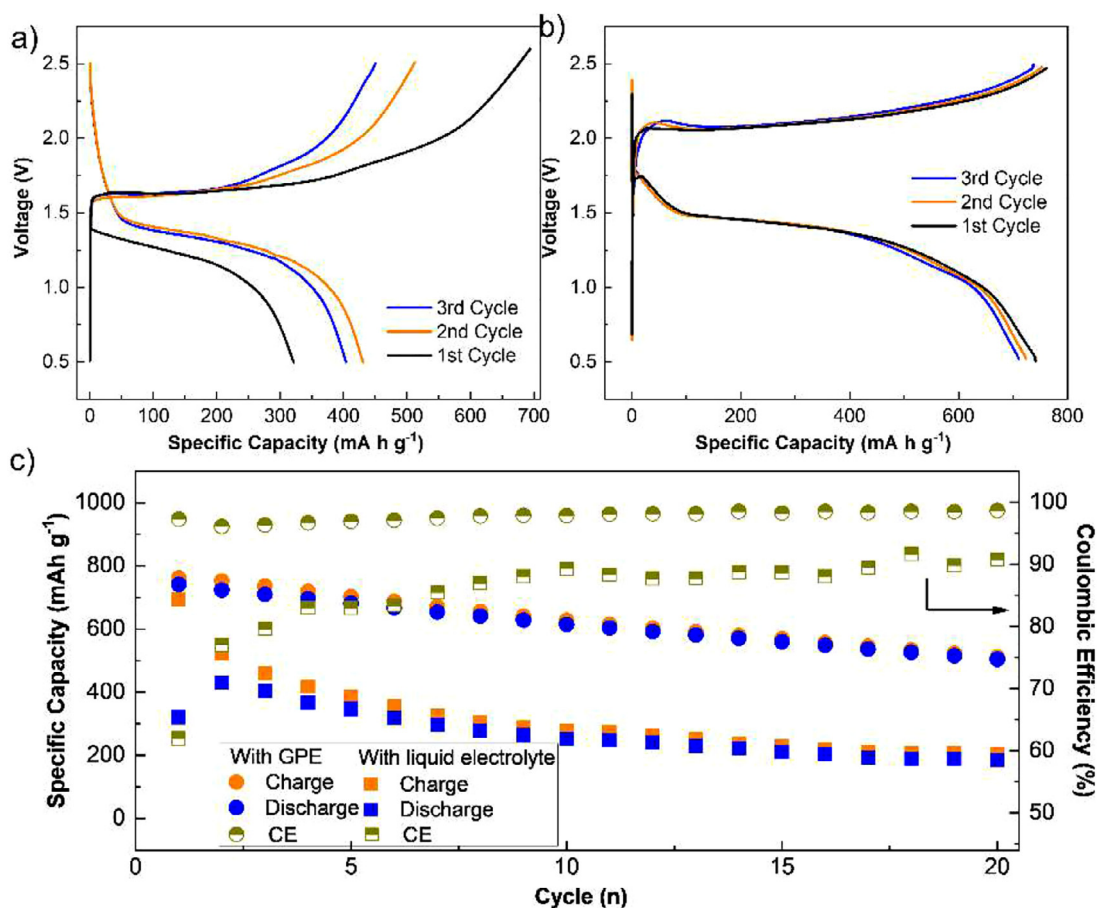
Fig. 5. Galvanostatic discharge/charge curves of the first three cycles of ACC/S cathode with (a) liquid electrolyte and (b) MgBOR−PTHF−GPE after rest under open-circuit conditions for 24 h. (c) The corresponding Coulombic efficiencies and cycling performance of Mg−S coin cells after rest for 24 h at a current density of 0.1C.

times the number of the cell with liquid electrolyte. In the 30th cycle, the discharge capacity of the cell with liquid electrolyte decreased to 122.7 mA h g^{-1}. Moreover, the cell kept over charging and broken down afterwards. These results suggest that GPE can limit the dissolution and diffusion of the polysulfide intermediates, thus preventing self discharge initiation. To visually demonstrate the effect of GPE on the suppression of polysulfide diffusion, two H type glass cells were assembled with a pristine glass fiber separator and a GPE filled separator. The tetraglyme solvent with and without magnesium polysulfide (MgS$_n$) solution was injected in the left and the right chamber, respectively. The procedure for the synthesis of MgS$_n$ solution can be found in the supporting infor mation. As shown in **Fig. S12**, in the H type cell with the blank separator (left), the red brown polysulfides gradually passed through the separa tor from left to right in the first three hours. In contrast, there is no obvious polysulfide diffusion observed from the cell with GPE separator (right). After 24 h, comparing to the cell with pristine separator, a much less color change can be seen in the cell with GPE, which confirms that the GPE can effectively suppress the polysulfide diffusion.

The CV performance of the Mg−S cell was also characterized with a three electrode cell. As shown in **Fig. 6**a, during the first cathodic scan, the main reduction peak emerged at around 1.22 V, while the oxidation peak appeared at around 2.00 V with respect to the Mg$_{RE}$ electrode. In the second cycle, both the cathodic and anodic signals shifted towards lower voltage polarization (1.31 V and 1.95 V, respectively). In parallel, the corresponding potentials *vs.* Mg$_{CE}$ were recorded. It showed a similar trend but higher overpotential, especially during the cathode oxidation, which is attributed to the energy barrier for Mg plating from GPE. These results are consistent with the plateaus in discharge/charge profiles (Fig.

6b). EIS was measured to provide further insight into the enhanced elec trochemical performance (Fig. 6c). The EIS spectra show a compressed semicircle in the high to medium frequency region of each spectrum, which is related to the interface impedance (R$_1$) and charge transfer resistance of the electrodes (R$_2$). The fitting results are summarized in **Table S2**. When cycling, both the interface and the charge transfer resis tance decreased sharply, which can be attributed to the good interfacial compatibility and high conductivity of MgBOR−PTHF−GPE. In addition, cycling performance is also displayed in Fig. 6d. At a current density of 0.1C, the discharge capacity of the first cycle was 897 mA h g^{-1}, and it remained at 228 mA h g^{-1} after 50 cycles. Besides, the Coulombic efficiency of the 1st cycle was 95% and it increased after the 2nd cycle. Meanwhile, the cycling performance of the cell with high sulfur load ing (~2.5 mg cm^{-2}) was also demonstrated in **Fig. S13**, which shows also a high Coulombic efficiency close to 100% after the 3rd cycle but a slightly less discharge capacity. The decreased capacity could be related to the slow kinetics of the sulfur redox reaction related to the high sulfur loading, which prevents the complete utilization of active material. In addition, the surface morphology and composition of the separator (**Fig. S14**) and anode (**Fig. S15**a−**16**) with GPE after cycling were examined by SEM and EDS analysis. The SEM images show that on the separator the MgBOR−PTHF−GPE was still uniformly distributed, indicating the robustness of the GPE. From the EDS analysis of the anode side, the Mg anode was covered with MgBOR−PTHF−GPE after 30 cycles. The ab sence of sulfur on the Mg anode side further confirms a good blockage capability of MgBOR−PTHF−GPE for polysulfide through the separator, thus inhibiting the passivation of the Mg anode. In contrast, in case of liquid electrolyte, sulfur can be detected on the Mg anode after cycling
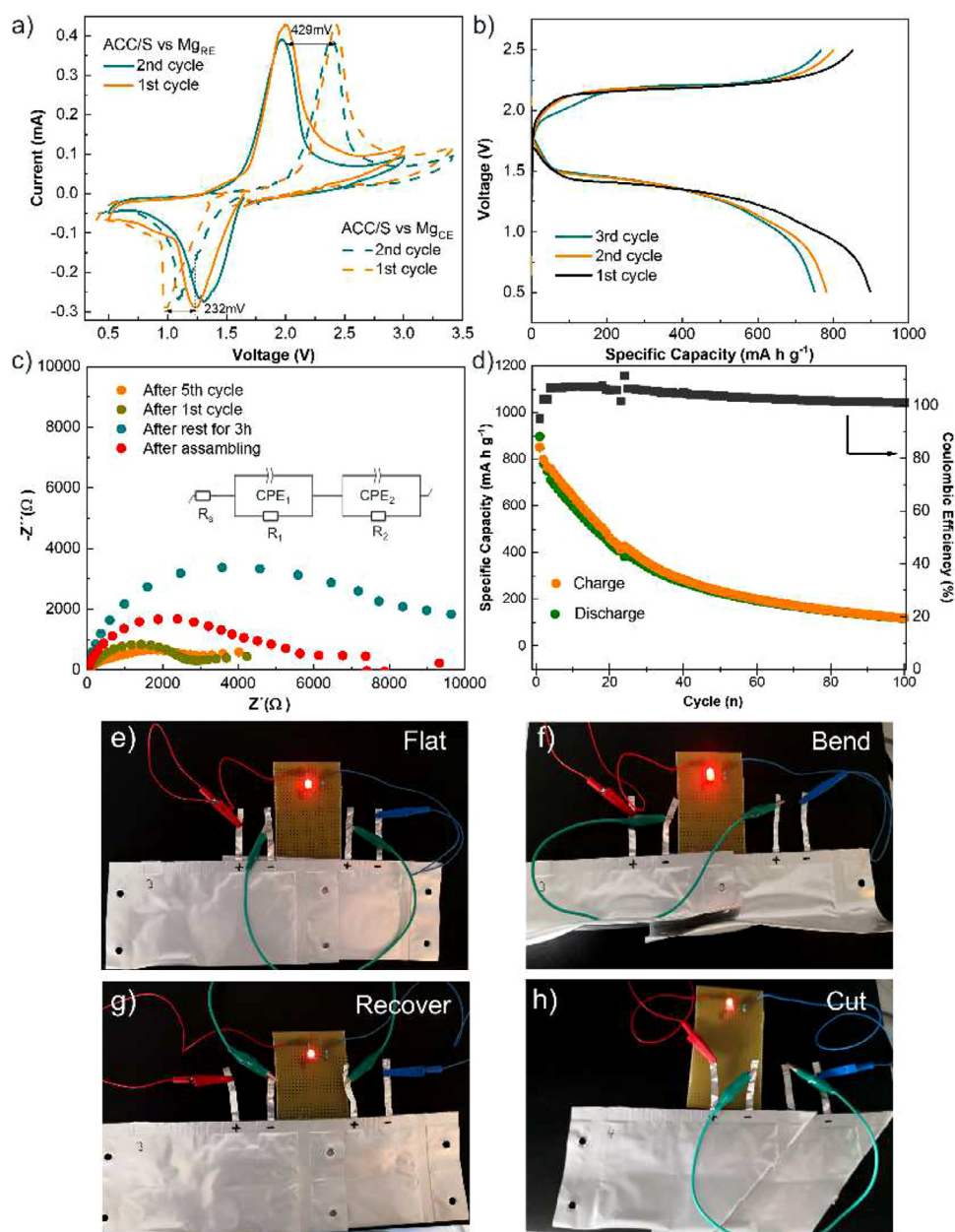
Fig. 6. (a) CVs of ACC/S//MgBOR−PTHF−GPE//Mg cells with a three-electrode setup with a scan rate of 0.1 mV s^{-1} for the first two cycles. (b) Galvanostatic discharge/charge curves of the first three cycles. (c) Nyquist plots of the cell before cycling, after 1st and 5th cycles. (d) Cycling performance of cells at a current density of 0.1C. (e-h) Optical images of LED lamps lighted by pouch cells under various mechanical deformations.

(Figure S15b and **Fig. 17**). The further results of Mg anode in the cell with MgBOR−PTHF−GPE after 100 cycles are displayed in **Fig. S18**.

To further demonstrate the gel electrolyte in a more practical cell configuration, Ketjen black/S//MgBOR−PTHF−GPE//Mg pouch cells were assembled with 50×50 mm^2 cathode sheets. More details about pouch cell are described in the supporting information. Pouch cells were cycled at a current of 0.05C as shown in **Fig. S19**. The power delivery exhibits no failure regardless of the changes of either bending or even cutting (Fig. 6e h). This can be attributed to GPE, which contributes to improvements in safety issues, including less internal short circuit and less electrolyte leakage. The result further confirms that the gel elec trolyte can be used on a large scale application for developing quasi solid state battery systems.

2.3. MgBOR−PETEA−GPE for Mg−S batteries

To further verify this concept, the Mg[B(hfip)$_4$]$_2$ based GPE is ex tended to the other polymer backbone, for example, using pentaery thritol tetraacrylate (PETEA) as monomer, which is reported in some other metal−sulfur systems [54,55]. Azobisisobutyronitrile (AIBN) was used to initiate the polymerization of PETEA as illustrated in **Fig. 7**a. The polymerization reaction occurs in liquid electrolyte and the MgBOR−PETEA−GPE is thus obtained. From FTIR spectra in **Fig. S20**, the C=C double bond (1630 cm^{-1}) of the PETEA monomer al most disappears after the formation of GPE, indicating the polymer ization of PETEA monomers. The electrochemical properties of the MgBOR−PETEA−GPE were characterized as displayed in **Fig. S21**. The ionic conductivity was calculated to be 3.42 ($\pm$ 0.04) mS cm^{-1} and $t_{Mg^{2+}}$ of MgBOR−PETEA−GPE was determined to be $t_+ = 0.394 \pm 0.02$. Details can be found in the supporting information. The GPE was formed on sep arator and characterized by SEM (Fig. 7b). As shown in the SEM image, the separator was fully covered with GPE. A similar self discharge test was carried out for 48 h under OCV with a three electrode cell (Fig. 7c). The potential of both the working and the counter electrodes are stable, for example, E_{we} increased from 1.82 V to 1.89 V after 48 h. The stable OCV confirms that although changing the polymer backbone, the GPE can still effectively suppress the self discharge. The discharge/charge curves of the first three cycles are almost overlapped with less capacity
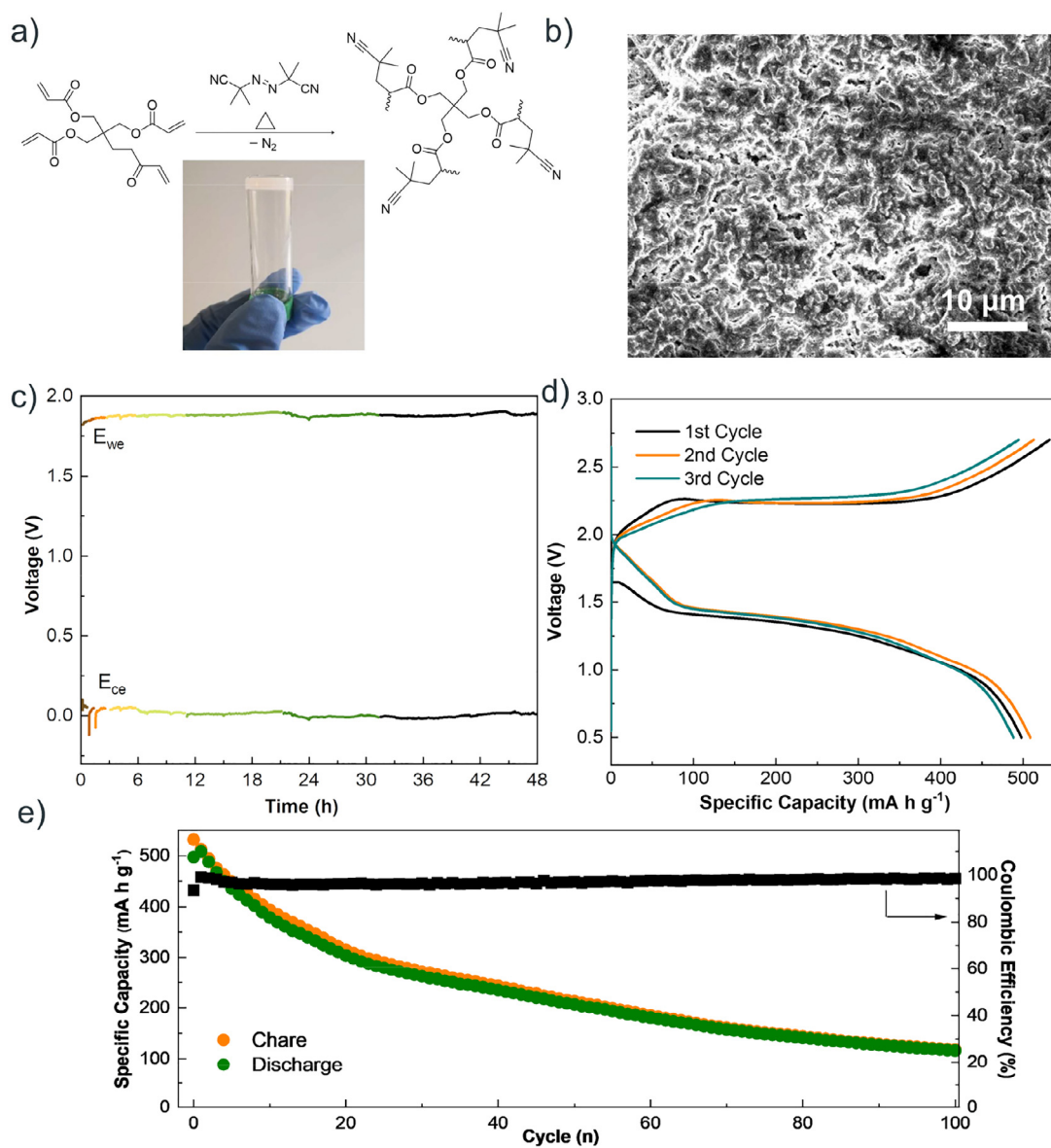
Fig. 7. (a) Optical photograph and the polymerization reaction of MgBOR−PETEA−GPE. (b) SEM image of glass fiber membrane coated with dry MgBOR−PETEA−GPE. (c) Potential profiles of the Mg−S cell with a three-electrode setup kept at OCV over 48 h. (d) Galvanostatic discharge/charge curves of ACC/S//MgBOR−PETEA−GPE//Mg cells during the first three cycles and (e) the corresponding cycling performance at a current density of 0.1C.

loss as presented in Fig. 7d. At a current density of 0.1C, the discharge capacity of the first cycle was 497.8 mA h g^{-1} with a Coulombic efficiency of 93.6%, and it remained at 208.7 mA h g^{-1} after 50 cycles. Besides, the Coulombic efficiency increased to 99.1% after the 2nd cycle and kept stable up to 100 cycles (Fig. 7e). Comparing to liquid electrolyte, both GPEs show much improved Coulombic efficiencies, which attributes to the unique structure of GPE. The initial capacity of this cell is lower than the cell with MgBOR−PTHF−GPE at room temperature. When using an increased operating temperature, the initial capacity increased above 1000 mA h g^{-1} (**Fig. S22**). It can be explained by the different wetting behaviors of GPEs on the cathode, which leads to the difference in sulfur utilization. Meanwhile, the capacity retention and Coulombic efficiency are related to the capability of the polymer network for trapping the solvent and some interactions between electrodes and GPEs. Overall, combining the advantages of polymer backbone and magnesium salt, both MgBOR−PETEA/PTHF−GPEs demonstrate good electrochemical properties and compatibility. These results manifest that the Mg[B(hfip)$_4$]$_2$ based GPEs can be extended to different polymer backbones.

Further works are required to improve the capacity retention of the battery, which may relate to some irreversible blockage of the active material in the GPE. And some operando characterizations may help us figure out the electrochemical process inside the GPE and the degradation during cycling in Mg−S cells. All the results in this work validate that Cl free Mg[B(hfip)$_4$]$_2$ based GPEs can provide a good Mg^{2+} conductivity, low interface resistance, and good compatibility with sulfur cathode. The electrochemical performance is noteworthy in the quasi solid state Mg−S battery and the concept will serve as a new chance for further optimization of the Mg−S system.

3. Conclusion

In conclusion, a new type of Mg[B(hfip)$_4$]$_2$ based gel polymer electrolyte has been developed via a straightforward and scalable *in situ* reaction in DME. To our knowledge, this is the first gel polymer electrolyte, which is capable of reversible Mg plating/stripping and compatible with a sulfur cathode up to date. Its good electrochemical properties and the polymeric characteristics enable stable cycling performance of

both conventional insertion and sulfur cathodes in Mg batteries. In particular, the GPE can simultaneously serve as a blocking layer for polysulfide, which offering new exploration direction for Mg S batteries. Furthermore, the GPE can be simply prepared from a liquid electrolyte and easily integrated into devices, which opens a new avenue for the development of magnesium batteries.

Data Availability

No data was used for the research described in the article.

References

[1] T.D. Gregory, R.J. Hoffman, R.C. Winterton, J. Electrochem. Soc. 137 (1990) 775.
[2] J.O. Besenhard, M. Winter, ChemPhysChem 3 (2002) 155–159.
[3] H.D. Yoo, I. Shterenberg, Y. Gofer, G. Gershinsky, N. Pour, D. Aurbach, Energy Environ. Sci. 6 (2013) 2265–2279.
[4] R. Mohtadi, F. Mizuno, Beilstein J. Nanotechnol. 5 (2014) 1291–1311.
[5] Y. Zhang, H. Geng, W. Wei, J. Ma, L. Chen, C.C. Li, Energy Storage Mater 20 (2019) 118–138.
[6] R. Deivanayagam, B.J. Ingram, R. Shahbazian-Yassar, Energy Storage Mater 21 (2019) 136–153.
[7] R. Mohtadi, O. Tutusaus, T.S. Arthur, Z. Zhao-Karger, M. Fichtner, Joule 5 (2021) 581–617.
[8] B. Park, J.L. Schaefer, J. Electrochem. Soc. (2020) 167.
[9] H.S. Kim, T.S. Arthur, G.D. Allred, J. Zajicek, J.G. Newman, A.E. Rodnyansky, A.G. Oliver, W.C. Boggess, J. Muldoon, Nat. Commun. 2 (2011) 427.
[10] J. Luo, S. He, T.L. Liu, ACS Energy Lett 2 (2017) 1197–1202.
[11] A. Du, Z. Zhang, H. Qu, Z. Cui, L. Qiao, L. Wang, J. Chai, T. Lu, S. Dong, T. Dong, H. Xu, X. Zhou, G. Cui, Energy Environ. Sci. 10 (2017) 2616–2625.
[12] W. Li, S. Cheng, J. Wang, Y. Qiu, Z. Zheng, H. Lin, S. Nanda, Q. Ma, Y. Xu, F. Ye, M. Liu, L. Zhou, Y. Zhang, Angew. Chem. Int. Ed. 55 (2016) 6406–6410.
[13] S. Yagi, A. Tanaka, Y. Ichikawa, T. Ichitsubo, E. Matsubara, J. Electrochem. Soc. 160 (2013) C83–C88.
[14] R. Attias, M. Salama, B. Hirsch, Y. Goffer, D. Aurbach, Joule 3 (2019) 27–52.
[15] O. Tutusaus, R. Mohtadi, T.S. Arthur, F. Mizuno, E.G. Nelson, Y.V. Sevryugina, Angew. Chem. Int. Ed. 54 (2015) 7900–7904.
[16] J.T. Herb, C.A. Nist-Lund, C.B. Arnold, ACS Energy Lett 1 (2016) 1227–1232.
[17] W. Ren, D. Wu, Y. NuLi, D. Zhang, Y. Yang, Y. Wang, J. Yang, J. Wang, ACS Energy Lett 6 (2021) 3212–3220.
[18] Z. Zhao-Karger, M.E. Gil Bardaji, O. Fuhr, M. Fichtner, J. Mater. Chem. A 5 (2017) 10815–10820.
[19] Z. Zhao-Karger, R. Liu, W. Dai, Z. Li, T. Diemant, B.P. Vinayan, C. Bonatto Minella, X. Yu, A. Manthiram, R.J. Behm, M. Ruben, M. Fichtner, ACS Energy Lett 3 (2018) 2005–2013.
[20] J. Luo, Y. Li, H. Zhang, A. Wang, W.S. Lo, Q. Dong, N. Wong, C. Povinelli, Y. Shao, S. Chereddy, S. Wunder, U. Mohanty, C.K. Tsung, D. Wang, Angew. Chem. Int. Ed. 58 (2019) 15313–15317.
[21] J. Song, E. Sahadeo, M. Noked, S.B. Lee, J. Phys. Chem. Lett. 7 (2016) 1736–1749.
[22] Z. Zhao-Karger, M. Fichtner, Front. Chem. 6 (2018) 656.
[23] A. Robba, A. Vizintin, J. Bitenc, G. Mali, I. Arčon, M. Kavčič, M. Žitnik, K. Bučar, G. Aquilanti, C. Martineau-Corcos, A. Randon-Vitanova, R. Dominko, Chem. Mater. 29 (2017) 9555–9564.
[24] R. Richter, J. Häcker, Z. Zhao-Karger, T. Danner, N. Wagner, M. Fichtner, K.A. Friedrich, A. Latz, ACS Appl. Energy Mater. 4 (2021) 2365–2376.
[25] T. Gao, X. Ji, S. Hou, X. Fan, X. Li, C. Yang, F. Han, F. Wang, J. Jiang, K. Xu, C. Wang, Adv. Mater. 30 (2018) 1704313.
[26] R. Richter, J. Häcker, Z. Zhao-Karger, T. Danner, N. Wagner, M. Fichtner, K.A. Friedrich, A. Latz, ACS Appl. Energy Mater. 3 (2020) 8457–8474.
[27] H.O. Ford, E.S. Doyle, P. He, W.C. Boggess, A.G. Oliver, T. Wu, G.E. Sterbinsky, J.L. Schaefer, Energy Environ. Sci. 14 (2021) 890–899.
[28] C. Han, H. Li, R. Shi, T. Zhang, J. Tong, J. Li, B. Li, J. Mater. Chem. A 7 (2019) 23378–23415.
[29] B. Pan, D. Zhou, J. Huang, L. Zhang, A.K. Burrell, J.T. Vaughey, Z. Zhang, C. Liao, J. Electrochem. Soc. 163 (2016) A580–A583.
[30] L. Cui, L. Zhou, K. Zhang, F. Xiong, S. Tan, M. Li, Q. An, Y.-M. Kang, L. Mai, Nano Energy 65 (2019) 103902.
[31] B. Pan, J. Huang, Z. Feng, L. Zeng, M. He, L. Zhang, J.T. Vaughey, M.J. Bedzyk, P. Fenter, Z. Zhang, A.K. Burrell, C. Liao, Adv. Energy Mater. 6 (2016) 1600140.
[32] P. Saha, M.K. Datta, O.I. Velikokhatnyi, A. Manivannan, D. Alman, P.N. Kumta, Prog. Mater. Sci. 66 (2014) 1–86.
[33] A. Du, H. Zhang, Z. Zhang, J. Zhao, Z. Cui, Y. Zhao, S. Dong, L. Wang, X. Zhou, G. Cui, Adv. Mater. 31 (2019) 1805930.
[34] G.P. Pandey, R.C. Agrawal, S.A. Hashmi, J. Phys. D: Appl. Phys. 43 (2010) 255501.
[35] G.P. Pandey, R.C. Agrawal, S.A. Hashmi, J. Solid State Electrochem. 15 (2011) 2253–2264.
[36] G.P. Pandey, S.A. Hashmi, J. Power Sources 187 (2009) 627–634.
[37] R. Deivanayagam, M. Cheng, M. Wang, V. Vasudevan, T. Foroozan, N.V. Medhekar, R. Shahbazian-Yassar, ACS Appl. Energy Mater. 2 (2019) 7980–7990.
[38] J.-S. Oh, J.-M. Ko, D.-W. Kim, Electrochim. Acta 50 (2004) 903–906.
[39] L.C. Merrill, H.O. Ford, J.L. Schaefer, ACS Appl. Energy Mater. 2 (2019) 6355–6363.
[40] Y. Shao, N.N. Rajput, J. Hu, M. Hu, T. Liu, Z. Wei, M. Gu, X. Deng, S. Xu, K.S. Han, J. Wang, Z. Nie, G. Li, K.R. Zavadil, J. Xiao, C. Wang, W.A. Henderson, J.-G. Zhang, Y. Wang, K.T. Mueller, K. Persson, J. Liu, Nano Energy 12 (2015) 750–759.
[41] O. Chusid, Y. Gofer, H. Gizbar, Y. Vestfrid, E. Levi, D. Aurbach, I. Riech, Adv. Mater. 15 (2003) 627–630.
[42] H. Fan, Y. Zhao, J. Xiao, J. Zhang, M. Wang, Y. Zhang, Nano Research 13 (2020) 2749–2754.
[43] H.O. Ford, L.C. Merrill, P. He, S.P. Upadhyay, J.L. Schaefer, Macromolecules 51 (2018) 8629–8636.
[44] K.M. Anilkumar, B. Jinisha, M. Manoj, S. Jayalekshmi, Eur. Polym. J. 89 (2017) 249–262.
[45] E.M. Miner, S.S. Park, M. Dinca, J. Am. Chem. Soc. 141 (2019) 4422–4427.
[46] N.S. Schauser, R. Seshadri, R.A. Segalman, Mol. Syst. Des. Eng 4 (2019) 263–279.
[47] J. Evans, C.A. Vincent, P.G. Bruce, Polymer 28 (1987) 2324–2328.
[48] Z. Song, Z. Zhang, A. Du, S. Dong, G. Li, G. Cui, J. Energy Chem. 48 (2020) 299–307.
[49] H. Fan, Z. Zheng, L. Zhao, W. Li, J. Wang, M. Dai, Y. Zhao, J. Xiao, G. Wang, X. Ding, H. Xiao, J. Li, Y. Wu, Y. Zhang, Adv. Funct. Mater. (2019) 30.
[50] X. Zhao, Y. Yang, Y. NuLi, D. Li, Y. Wang, X. Xiang, Chem. Commun. 55 (2019) 6086–6089.
[51] B.P. Vinayan, H. Euchner, Z. Zhao-Karger, M.A. Cambaz, Z. Li, T. Diemant, R.J. Behm, A. Gross, M. Fichtner, J. Mater. Chem. A 7 (2019) 25490–25502.
[52] O. Tutusaus, R. Mohtadi, N. Singh, T.S. Arthur, F. Mizuno, ACS Energy Lett 2 (2017) 224–229.
[53] Z. Li, T. Diemant, Z. Meng, Y. Xiu, A. Reupert, L. Wang, M. Fichtner, Z. Zhao-Karger, ACS Appl. Mater. Interfaces 13 (2021) 33123–33132.
[54] M. Liu, D. Zhou, Y.-B. He, Y. Fu, X. Qin, C. Miao, H. Du, B. Li, Q.-H. Yang, Z. Lin, T.S. Zhao, F. Kang, Nano Energy 22 (2016) 278–289.
[55] Y. Ren, N. Hortance, J. McBride, K.B. Hatzell, ACS Energy Lett 6 (2021) 345–353.